Direct observation of spin-orbit-induced 3*d* hybridization via resonant inelastic extreme ultraviolet scattering on an edge-sharing cuprate

Marco Malvestuto,[1,2,*] Antonio Caretta,[1] Barbara Casarin,[2] Roberta Ciprian,[1,†] Martina Dell'Angela,[3] Simone Laterza,[2] Yi-De Chuang,[4] Wilfried Wurth,[5,6] Alexandre Revcolevschi,[7] L. Andrew Wray,[8] and Fulvio Parmigiani[1,2,9]

[1]*Elettra-Sincrotrone Trieste S.C.p.A. Strada Statale 14 - km 163.5 in AREA Science Park 34149 Basovizza, Trieste, Italy*

[2]*Department of Physics, University of Trieste, Via A. Valerio 2, 34127 Trieste, Italy*

[3]*CNR-IOM, Strada Statale 14 - km 163.5 in AREA Science Park 34149 Basovizza Trieste, Italy*

[4]*Advanced Light Source, Lawrence Berkeley National Laboratory, Berkeley, California 94720, USA*

[5]*Physics Department and Center for Free-Electron Laser Science, Hamburg University, 22607 Hamburg, Germany*

[6]*Photon Science, DESY, Notkestrasse 85, 22607 Hamburg, Germany*

[7]*Synthèse, Propriétés et Modélisation des Matériaux (SP2M) UMR 8182, Bat 410-415, Université Paris - Sud 91405 ORSAY Cedex, France*

[8]*Department of Physics, New York University, 4 Washington Place, New York, New York 10003, USA*

[9]*International Faculty, University of Cologne, 50937 Cologne, Germany*

(Received 4 December 2018; published 15 March 2019)

Using high resolution resonant inelastic x-ray scattering measurements, we have observed that the orbital excitations of the quasi-1D spin chain compound $CuGeO_3$ has nontrivial and noticeable orbital mixing effects from 3*d* valence spin-orbit coupling. In particular, the SOC leads to a significant correction of d_{z^2} state, which has a direct interplay with the low energy physics of cuprates. Guided by atomic multiplet based modeling, our results strongly support a 3*d* spin-orbit mixing scenario and explore in detail the nature of these excitations.

DOI: 10.1103/PhysRevB.99.115120

I. INTRODUCTION

Spin-orbit coupling originates many exotic properties of quantum materials [1–6]. Although small, SOC effect, often combined with electronic correlation, is visible all throughout 3*d* electron systems.

In cuprates, spin-orbit coupling is known to cause the Lande *g*-factor tensor for Cu^{2+} to deviate from 2 and it also leads to the Dzyaloshinski-Moriya antisymmetric exchange interaction, which underlies the spin canting and weak ferromagnetism in La_2CuO_4 [7].

Recently, the spin-orbit coupling constant of cuprate 3*d* electrons has been found to play a remarkably large role in defining electronic symmetries at the Fermi level and nontrivial spin texture [8] and underpinning predictions of current loop [9,10], topological spin liquid many-body phases, and spin polarizability of cuprate quasiparticles [11–13].

In the present work we explore the effects of the 3*d* valence SOC on the orbital excitations of an archetypical cuprate belonging to the quasi-one-dimensional (1D) edge-shared class of quantum magnets [14], $CuGeO_3$, by combining high resolution Cu M_{23} edge RIXS [15–17] and atomic multiplet (AM) calculations.

Crystal field excitations, which correspond to a local rearrangement of the 3*d* holes, play a crucial role in many properties of these materials and reveal the orbital energies that are fundamental to establishing microscopic theoretical models (e.g., tight binding). However, recent microscopically based models have drawn attention to 3*d* SOC as another key parameter mediating the interplay of orbital currents [18] with spin angular momentum, highlighting the importance of identifying not just the orbital excitation energies, but also this 3*d* SOC-mediated orbital symmetry mixing.

In the perspective of our results, $CuGeO_3$ [19–25] reveals itself as an intriguing case study about the effects of the 3*d* spin-orbit coupling (SOC) on the orbital excitation in cuprates. In fact, the orbital excitation in $CuGeO_3$ are closer together in energy with respect to other cuprates [26], and this promotes pronounced mixing effects from 3*d* valence SOC, which can affect the electronic ground state of the CuO_6 octahedron. Hence, the importance of this material stems from being a simple model sharing key physical behaviors with more complex two-dimensional cuprate materials.

We demonstrate that including SOC leads to a significant correction to the binding energy of d_{z^2}, which has a direct interplay with cuprate low energy physics as a parallel channel for oxygen p_σ hybridization. We also observe the energy loss drift in the d_{xz}, d_{yz}-derived RIXS feature, which is predicted when 3*d* SOC orbital mixing occurs. This in turn can also be seen as a slight structural distortion of the CuO_4 plaquette which can play a role in the low energy physics of $CuGeO_3$, and possibly of other similar cuprates.

II. EXPERIMENT

At room temperature, $CuGeO_3$ [27] has an orthorhombic cell with space group D_5-*Pbmm* with lattice parameters $a = 4.801$ Å, $b = 8.472$ Å, and $c = 2.942$ Å. The crystal structure [see Fig. 1(a)] is characterized by chains of edge-sharing CuO_6 octahedra units, where Cu^{2+} ions are at the center of a square of O^{-2} ions [O(1)], running along the *c* axis. Two

*marco.malvestuto@elettra.eu

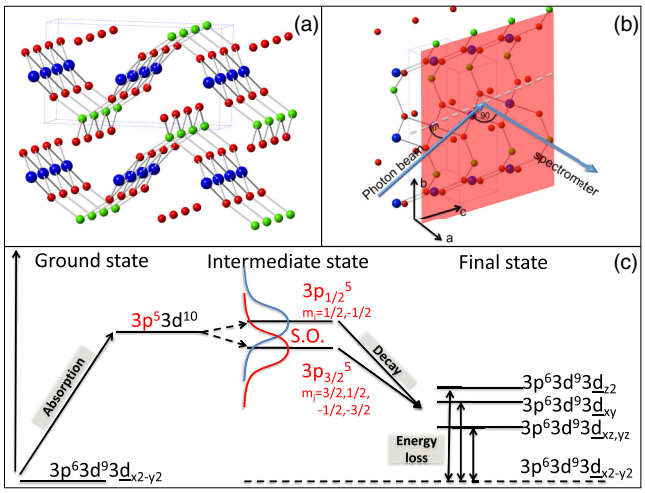

FIG. 1. (a) Crystal structure of $CuGeO_3$. (b) Schematic of the scattering geometry. The scattering plane, which includes the photon beam and the spectrometer, is perpendicular to the *bc* crystal plane. The photon polarization is in the scattering plane. (c) RIXS energy scheme for $3p$-$3d$ scattering channels. The vertical axis represents the energy of the electron configuration in arbitrary units. For simplicity only the shells which are changing in configuration are shown. A core-hole spin-orbit coupling separates in energy the [$3p_{1/2}$; $3p_{3/2}$] intermediate states, which are considerably overlapped due to lifetime broadening and thus it must be considered as a nonpure intermediate state. The final state is a superposition of ground state and orbital excitations.

apical weakly bonded oxygen are present above and below each plaquette to yield a strongly distorted CuO_6 octahedron, allowing for easy cleavage. The chains of edge-sharing CuO_4 units are connected along the *c* axis by corner-sharing units of Ge^{4+} ions tetrahedrally coordinated with in-plane and apical oxygen. Platelike samples were cleaved along the *b*-*c* axis as illustrated in Fig. 1(b). The cleaved surface is oriented perpendicular to the [100] axis, so that the buckle angle of the CuO_2 plaquette relative to the cleaved surface is 55.57°. The sample was a 200 μm thick single crystal $CuGeO_3$. The x-ray penetration depth at 74 eV is about 5 nm [28].

In RIXS, the resonant absorption of a photon by a core electron leads to a radiative de-excitation which leaves the system either in its ground or in a neutral excited state [29,30]. Thus *dd* excitations yield characteristic spectral losses dispersing with incident photon energy (Raman regime) and information is projected on the cation site [31,32]. Nowadays, high energy resolutions ($\leqslant$25 meV) can be achieved by RIXS spectrometers in the soft and hard x-ray regime [33–38]. However, extending the RIXS spectroscopy into an extreme ultraviolet (EUV) [39] regime can provide a wealth of benefits with respect to the soft x-ray energy range; for example, achieving superior energy resolution at moderate instrumentation resolving power and potentially offering simpler interpretations for the spectral features [39–42]. M_{23}-edge XAS and RIXS measurements were performed at the beamline 4.0.3 (MERLIN) RIXS endstation (MERIX) [38] at the Advanced Light Source (ALS), Lawrence Berkeley National Laboratory. The overall energy resolution was ~18 meV (FWHM). Local excitations with copper specificity can be measured by tuning the x-ray photon energies at the Cu $3p$ absorption edges (around 74–78 eV).

A schematic view of the RIXS scattering geometry is reported in Fig. 1(b). The incident polarization was linear, parallel to the horizontal scattering plane. The angle between the *bc* crystal plane and the incoming EUV beam is ~20°. The detector was placed in a direction perpendicular to the incident beam, which is a typical 90° scattering geometry with linearly polarized incoming x rays and no polarization analysis of the outgoing x rays. As inelastic scattering at the Cu $3p$ edges occurs only via excitation to the unoccupied $3d_{z^2}$, a projection of the polarization of the incident radiation is kept into the CuO_2 planes.

In order to model the experimental RIXS response of $CuGeO_3$, an atomic multiplet (AM) theory [39,43,44] approach has been used. The theoretical spectra have been calculated starting from a set of crystal field parameters ($10D_q$ = 1.62, $Dt = 0.1525$, and $Ds = 0.2856$) extracted from the experimental *d*-*d* energy positions. The extraction method of the crystal field parameters is discussed in the Supplemental Material [45].

III. DATA AND DISCUSSION

In $CuGeO_3$, the *d*-*d* excitations can be probed by the coherent photon absorption → re-emission transition sequence $3p^6 3d^9 3\bar{d}_{x^2-y^2}$(ground state) → $3p^5 d^{10}$(intermediate state) → $3p^6 3d^9$(final state). The transitions involved are shown in Fig. 1(c) as an energy level diagram.

In more detail, there are two types of orbital excitations in $CuGeO_3$: one excitation is a transition of an electron from the t_{2g} orbital to the e_g orbital (t_{2g} excitation) and the other one is between the e_g orbitals (e_g excitation). Following the absorption of a photon, of energy $h\nu$, an electron is promoted from a $3p$ orbital to the $3d$ shell, creating a $3p^5_{1/2,3/2}3d^{n+1}$ intermediate state. Intermediate states of Cu^{2+} have full $3d^{10}$ orbital occupation. In an atomic multiplet picture, the $3p^5_{1/2,3/2}3d^{10}$ state is made of two intermediate states with different spin-orbit symmetries: $J = 3/2$ (M_3) and $J = 1/2$ (M_2). When these intermediate states decay and the $3p$ core hole is filled, a photon of energy $h\nu'$ is emitted leaving the system with a $3d$ hole, whose orbital symmetry can be different from the ground state orbital symmetry.

The energy difference between this final state and the initial state is the overall energy transfer of the system. The visible RIXS features represent excited states in which a hole has been moved to a different orbital. Each excitation is labeled by the *d*-orbital symmetry of the hole. At the *M* edges, the $3p$ core-hole spin-orbit separation is comparable to the core-hole lifetime broadening. The core-hole SO is measured as the energy difference between the M_2 and M_3 edges and it is 2.41 eV. The core-hole lifetime width (1.6 eV; ~0.4 fs) is calculated as the FWHM of one of the deconvolved Lorentian RIXS peak feature. This leads to a nonpure intermediate state, which gives rise to quantum interference effects between the spin-orbit separated core states $3p^5_{1/2,3/2}3d^{10}$. In brief, after the photon absorption, the intermediate state remains in a coherent quantum superposition $|\psi\rangle = A|3p^5_{1/2}\rangle + B|3p^5_{3/2}\rangle$ (A and B are constants that hold the phase) with a lifetime

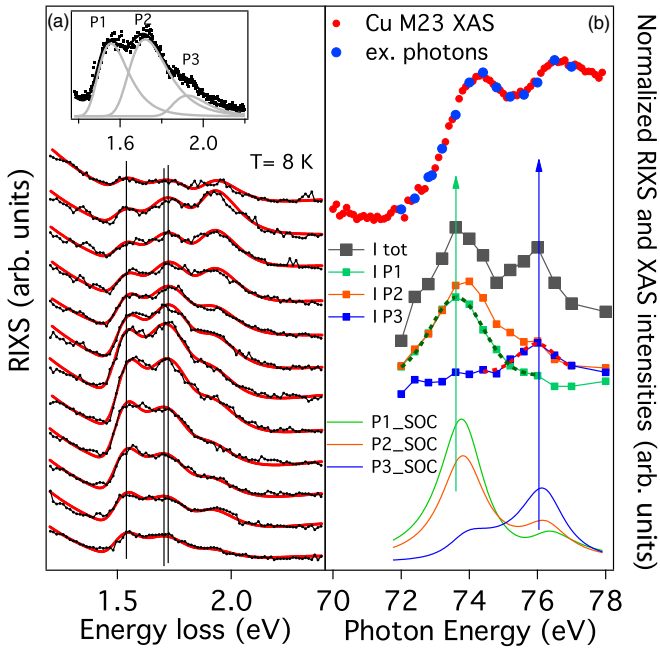

FIG. 2. High resolution Cu $M_{2,3}$ RIXS spectra are displayed in (a) (black curves). Three energy-loss peaks (P_1, P_2, P_3) representing d-d excitations are visible. An example of the fitting deconvolution of the d-d energy region of a RIXS spectrum measured at $h\nu =$ 74 eV is also shown in the inset of (a). Gray curves show the results of the fitting deconvolution. The fitting functions (red curves) of the RIXS spectra for all the excitation photon energies across the Cu M_{23} edge are displayed in (a) superimposed to the experimental data. (b) The experimental Cu $M_{2,3}$ XAS edge (red dotted curve) and the RIXS excitation photon energies (blue squares). The resonant intensities of the three distinct d-d features (P_1, P_2, P_3), their total intensity (black squared curve) and their theoretical calculated line shapes (colored continues lines) are displayed as a function of the incoming photon energies. The total RIXS intensity represents the total probability of a d-d excitation.

of few femtoseconds (core-hole lifetime). Depending on the relative phase between $|3p^5_{1/2}\rangle$ and $|3p^5_{3/2}\rangle$, the two states can interfere constructively or destructively giving rise to distinctive resonant line shapes of the RIXS intensities [42]. The pattern of interference is different for different final states, as it also depends on how the phase changes when going from the $|3p^5_{1/2}\rangle$ and $|3p^5_{3/2}\rangle$ states to a specific final state.

The measured Cu $3p$ RIXS spectra plotted over the 1.2–2.4 eV energy loss range are shown in Fig. 2(a). The excitation photon energies are reported in Fig. 2(b) (blue circles) superimposed to the Cu $M_{2,3}$ XAS spectrum. The energy position of the elastic component is kept at zero energy loss (0 eV). The spectra are normalized to the elastic peak. The spectra are measured at a temperature of 8 K for minimizing the thermal broadening. The elastic peak has a full width at half maximum of 18 meV, which is the resolution of the experiment. Three inelastic peaks are resolved in Fig. 2 at 1.56 eV (P_1), 1.75 eV (P_2), and 1.95 eV (P_3), which corresponds to excitations from the copper $3d_{x^2-y^2}$ hole ground state to orbitals of $3d_{xy}$, $3d_{xz/yz}$, and $3d_{z^2}$ symmetry [Fig. 1(c)].

The Cu $M_{2,3}$ XAS spectrum exhibits multiplet structures which are characterized by a prominent double peaked absorption band in the 72–78 eV energy region with a spin-orbit energy separation of 2.41 eV. These spectra are qualitatively similar to those of Cu oxides, which suggests that the $M_{2,3}$ absorption in $CuGeO_3$ are mainly due to intra-atomic transitions ($3p \rightarrow 3d$) within the metal ion.

In order to interpret the resonant behavior of the Cu d-ds, the RIXS multipeaked feature has been decomposed by a Lorentzian deconvolution [inset in Fig. 2(a)] and their intensities are plotted as a function of the excitation photon energies [colored square dot curves, Fig. 2(b)]. The sum of the single RIXS intensities is also displayed (black square dot curve), which gives the total probability that an orbital excitation of any symmetry is excited. The asymmetric excitation line shapes of the decomposed RIXS features accounts contributions from shake-up process in a fashion analogous to a generalized Frank-Condon picture as already reported and discussed in L-edge [41,46] and M-edge literature [42]. We note that the far weaker core hole effective monopole perturbation at the M edge provides a cleaner measurement in which one can neglect the incident energy dependence present in this line shape at the L edge.

The three inelastic components display a clear resonant character, while individual excitation modes show distinctive dependence on the incident photon energy. The two lowest energy peaks [$P_{1,d_{xy}}$ and $P_{2,d_{xz,yz}}$, green and yellow curves in Fig. 2(b)], which stems from a $t_{2g} \rightarrow e_g$ intraband transition, primarily resonate across the Cu $3p_{3/2}$ M_3 edge around 73.8 eV. In addition, the photon energy dependence of the intensity of $P_{2,d_{xz,yz}}$ displays a double peaked structure with a second weak resonance around the M_2 edge at 76 eV, which can be ascribed to a quantum interference pattern. On the contrary, the resonant character of the $P_{3,d_{z^2}}$ peak is enhanced when the excitation photon energy ranges over the Cu $3p_{1/2}$ M_2 edge. For the P_3 feature, which stems from the $3\bar{d}_{x^2-y^2} \rightarrow 3\bar{d}_{z^2}$ excitation, most of the spectral weight comes from spin flipped final states [44,47]. These final states technically occur via an "indirect RIXS" process associated with destructive interference between M_2 and M_3 resonance channels [42]. Spin-flip states consist of spin excitations localized on the scattering site and allowed by the resonant scattering through specific intermediate states. The reason this spin flip happens is due to the fact that the core hole $j = 3/2$ [red curve, Fig. 1(c)] and $j = 1/2$ [blue curve, Fig. 1(c)] states in the intermediate state are separated by the spin-orbit coupling and the spin is no longer a good quantum number. In principle, spin-flip states are expected to be shifted to higher energies by the exchange interaction. However, susceptibility measurements and low-lying spin excitation spectrum gave exchange constant values of $J = 7.58$ [48] and 10.4 meV [49], and the expected energy shift would be below the energy resolution of the present investigation. In this respect, $3d$ SOC is also needed for the $3d_{z^2}$ feature to be visible. This is because core spin-orbit coupling originate the spin flip, but will not allow the $3\bar{d}_{z^2} \rightarrow 3\bar{d}_{x^2-y^2}$ orbital transition. One needs $3d$ orbital symmetry mixing, which comes from the $3d$ SOC parameter.

The experimental RIXS quantum interference patterns are rather different but are quite well reproduced by the calculated

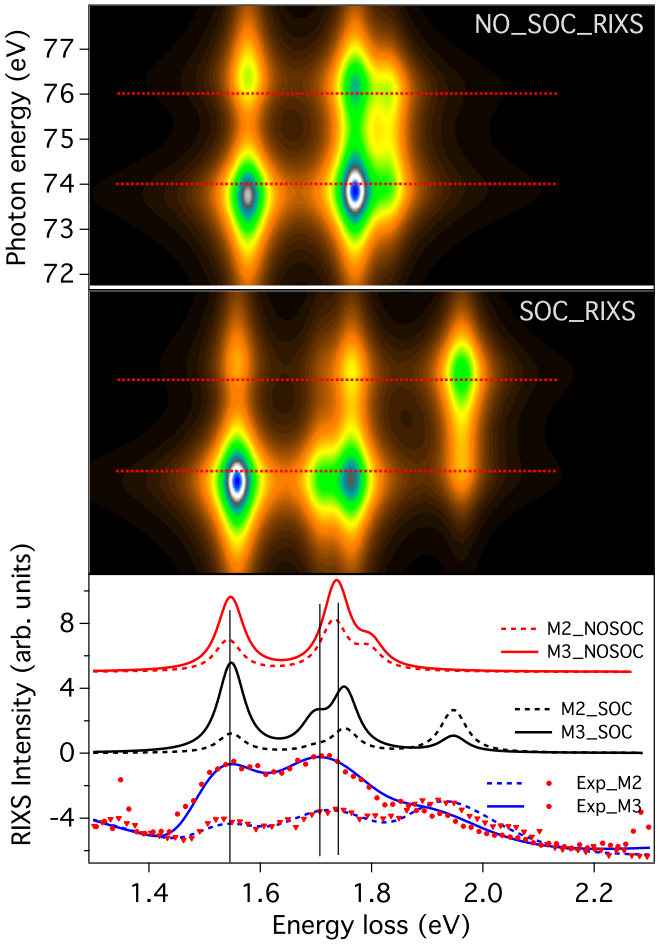

FIG. 3. Top and middle panels: Calculated Cu $M_{2,3}$ RIXS planes from $CuGeO_3$ in which the $3d$ SOC (0.102 eV) has been turned off/on respectively. The RIXS maps are displayed as a function of the incident photon energy and the energy loss of the scattered photon. The crystal field parameters used for the calculation are reported in Table I. The spin-orbit M_2/M_3 separation (2.41 eV) and the lifetime broadening (1.6 eV) are derived from the experiment. Bottom panel compares the simulated RIXS spectra (with/without $3d$ SOC) sliced from the maps at $h\nu = 74.4$ and 76.8 eV with the fitting curves of the experimental spectra (blue curves).

patterns, which we have reported in Fig. 2(b) (continuous colored curves) for comparison with the experimental data. The theoretical quantum interference patterns are slices of the theoretical RIXS maps (displayed in Fig. 3) taken at constant energy losses and corresponding to the three $P_{1,2,3}$ features.

Figure 3(a) displays the calculated RIXS maps over the excitation photon energies crossing the M_{23} edges and the photon energy loss with and without the $3d$ SOC mixing. The $3d$ SOC parameter (102 meV) has been calculated from Hartree-Fock numerics. The calculated spectra were broadened to mimic the experimental resolution. The AM calculation reveals that the P_2 feature, which experimentally appears to be a single feature, is actually made of two spin-orbit split features with different spin-orbit symmetries (d_{xz} and d_{yz}), whose energy separation is of the order of 50 meV (see Table I). In addition, the two spin-orbit split features appear to

TABLE I. The binding energies of the three d-d states ($P_{1,d_{xy}}$, $P_{2,d_{xz,yz}}$, and $P_{3,d_{x^2-y^2}}$) from this work are reported as calculated by the deconvolution procedure described in the text. The table reports the orbital binding energies from the AM calculation with and without the $3d$-SOC correction.

AM parameters				
		P_1	P_2	P_3
Expt. d-d BE (eV)		1.56	1.75	1.95
	x^2-y^2	xy	xz/yz	z^2
Orbital only (eV)	0	1.58	1.77	1.832
Orbital + SOC	0	1.56	1.711	1.95
			1.756	

resonate differently at the two M edges. In particular, the two features resonates simultaneously when crossing the M_3 edge, while the higher energy loss peak $P_{2,xz}$ resonates better at M_2 edge. Accordingly, the combined P_2 feature should appear to drift up slightly in energy as the incident photon energy is raised across the absorption edge.

Two sets of two slices of the calculated RIXS maps corresponding to the M_3 and M_2 photon energies are displayed as energy loss spectra in the bottom panel of Fig. 3 and qualitatively compared to the experimental spectra, which are nicely reproduced by the calculated RIXS spectra with SO coupling included. Since the predicted energy loss drift of the $d_{xz,yz}$ is at the limit of the energy resolution of the present RIXS experiment, our experimental results are not concluding. However, based on the results of the fitting deconvolution, an apparent shift of the spectral weight is found of about 40 meV within the limits of the experimental resolution.

IV. CONCLUSIONS

In conclusion, we have carried out a comprehensive high-resolution Cu M_{23} edge RIXS study of the $3d$ orbital excitations in the quantum magnet $CuGeO_3$. Thanks to finely resolved RIXS measurements, we succeeded to resolve the energy dependence of the d-d states across the Cu M_{23} edge.

Although the system has a modest $3d$ SOC, i.e., 102 meV, in agreement with literature [50], the high confidence in determining the crystal field parameters combined with calculated atomic multiplet RIXS spectra revealed pronounced mixing effects of the orbital states from $3d$ valence SOC. These effects include a significant binding energy correction to the d_{z^2} orbital, which has a direct interplay with cuprate low energy physics as a parallel channel for oxygen p_σ hybridization. A more accurate d_{z^2} energy is also found with respect to previous calculations [23]. We have also observed the energy loss drift in the xz/yz-derived P_2 feature, that, to the best of our knowledge, has never been reported for $CuGeO_3$. Our findings demonstrate that the $3d$ SOC play a remarkably large role in defining the picture of orbital excitations in cuprates. Accordingly, we also prove that the RIXS cross section is sensitive to the $3d$ SOC. We show that the improved energy resolution in RIXS spectroscopy will enable the detection of spectral signatures of low energy interactions and is essential for understanding the correlated nature of quantum materials

ACKNOWLEDGMENTS

This research used resources of the Advanced Light Source, which is a DOE Office of Science User Facility under Contract No. DE-AC02-05CH11231. Support by the Deutsche Forschungsgemeinschaft through the collaborative research center SFB925/project B2 is gratefully acknowledged.

[1] X.-L. Qi and S.-C. Zhang, Phys. Today **63**(1), 33 (2009).
[2] J. E. Moore, Nature (London) **464**, 194 (2010).
[3] D. Pesin and L. Balents, Nat. Phys. **6**, 376 (2010).
[4] S. Nakosai, Y. Tanaka, and N. Nagaosa, Phys. Rev. Lett. **108**, 147003 (2012).
[5] W. Witczak-Krempa, G. Chen, Y. B. Kim, and L. Balents, Annu. Rev. Condens. Matter Phys. **5**, 57 (2014).
[6] J. G. Rau, E. K.-H. Lee, and H.-Y. Kee, Annu. Rev. Condens. Matter Phys. **7**, 195 (2016).
[7] M. A. Kastner, R. Birgeneau, G. Shirane, and Y. Endoh, Rev. Mod. Phys. **70**, 897 (1998).
[8] K. Gotlieb, C.-Y. Lin, M. Serbyn, W. Zhang, C. L. Smallwood, C. Jozwiak, H. Eisaki, Z. Hussain, A. Vishwanath, and A. Lanzara, Science **362**, 1271 (2018).
[9] V. Aji and C. M. Varma, Phys. Rev. B **75**, 224511 (2007).
[10] M. E. Simon and C. M. Varma, Phys. Rev. Lett. **89**, 247003 (2002).
[11] N. Harrison, B. J. Ramshaw, and A. Shekhter, Sci. Rep. **5**, 10914 (2015).
[12] B. Lau, M. Berciu, and G. A. Sawatzky, Phys. Rev. Lett. **106**, 036401 (2011).
[13] I. Santoso, W. Ku, T. Shirakawa, G. Neuber, X. Yin, M. Enoki, M. Fujita, R. Liang, T. Venkatesan, G. A. Sawatzky, A. Kotlov, S. Yunoki, M. Rübhausen, and A. Rusydi, Phys. Rev. B **95**, 165108 (2017).
[14] G. Castilla, S. Chakravarty, and V. J. Emery, Phys. Rev. Lett. **75**, 1823 (1995).
[15] L. J. P. Ament, M. van Veenendaal, T. P. Devereaux, J. P. Hill, and J. van den Brink, Rev. Mod. Phys. **83**, 705 (2011).
[16] J. Schlappa, K. Wohlfeld, K. J. Zhou, M. Mourigal, M. Haverkort, V. N. Strocov, L. Hozoi, C. Monney, S. Nishimoto, S. Singh, A. Revcolevschi, J. S. Caux, L. Patthey, H. M. Rønnow, J. Van Den Brink, and T. Schmitt, Nature (London) **485**, 82 (2012).
[17] J. Schlappa, T. Schmitt, F. Vernay, V. N. Strocov, V. Ilakovac, B. Thielemann, H. M. Rønnow, S. Vanishri, A. Piazzalunga, X. Wang, L. Braicovich, G. Ghiringhelli, C. Marin, J. Mesot, B. Delley, and L. Patthey, Phys. Rev. Lett. **103**, 047401 (2009).
[18] V. Scagnoli, U. Staub, Y. Bodenthin, R. A. de Souza, M. García-Fernández, M. Garganourakis, A. T. Boothroyd, D. Prabhakaran, and S. W. Lovesey, Science **332**, 696 (2011).
[19] M. Bassi, P. Camagni, R. Rolli, G. Samoggia, F. Parmigiani, G. Dhalenne, and A. Revcolevschi, Phys. Rev. B **54**, R11030 (1996).
[20] S. D. Dević, Z. V. Popović, A. Breitschwerdt, G. Dhalenne, and A. Revcolevschi, Phys. Status Solidi B **203**, 579 (1997).
[21] C. de Graaf and R. Broer, Phys. Rev. B **62**, 702 (2000).
[22] S. Pagliara, F. Parmigiani, P. Galinetto, A. Revcolevschi, and G. Samoggia, Phys. Rev. B **66**, 024518 (2002).
[23] H.-Y. Huang, N. A. Bogdanov, L. Siurakshina, P. Fulde, J. v. d. Brink, and L. Hozoi, Phys. Rev. B **84**, 235125 (2011).
[24] D. Nardi, Time-resolved optical spectroscopy of $CuGeO_3$, Ph.D. thesis, Università Cattolica del Sacro Cuore Brescia, Italy, 2006.
[25] C. Giannetti, G. Zgrablic, C. Consani, A. Crepaldi, D. Nardi, G. Ferrini, G. Dhalenne, A. Revcolevschi, and F. Parmigiani, Phys. Rev. B **80**, 235129 (2009).
[26] M. M. Sala, V. Bisogni, C. Aruta, G. Balestrino, H. Berger, N. B. Brookes, G. M. De Luca, D. Di Castro, M. Grioni, M. Guarise, P. G. Medaglia, F. M. Granozio, M. Minola, P. Perna, M. Radovic, M. Salluzzo, T. Schmitt, K. J. Zhou, L. Braicovich, and G. Ghiringhelli, New J. Phys. **13**, 043026 (2011).
[27] G. Dhalenne, A. Revcolevschi, J. C. Rouchaud, and M. Federoff, Mater. Res. Bull. **32**, 939 (1997).
[28] The center for x-ray optics at lawrence berkeley national laboratory, http://www.cxro.lbl.gov/.
[29] A. Kotani and S. Shin, Rev. Mod. Phys. **73**, 203 (2001).
[30] J.-E. Rubensson, J. Lüning, S. Eisebitt, and W. Eberhardt, Appl. Phys. A **65**, 91 (1997).
[31] S. Tanaka and A. Kotani, J. Phys. Soc. Jpn. **62**, 464 (1993).
[32] S. Butorin, J. Guo, M. Magnuson, P. Kuiper, and J. Nordgren, Phys. Rev. B **54**, 4405 (1996).
[33] SIX Beamline: Soft Inelastic X-ray Scattering, Brookhaven National Laboratory, https://www.bnl.gov/ps/beamlines/beamline.php?r=2-ID.
[34] I21 Beamline, Diamond Light Source, http://www.diamond.ac.uk/Beamlines/Spectroscopy/I21.html.
[35] Y. V. Shvyd'ko, J. P. Hill, C. A. Burns, D. S. Coburn, B. Brajuskovic, D. Casa, K. Goetze, T. Gog, R. Khachatryan, J.-H. Kim, C. N. Kodituwakku, M. Ramanathan, T. Roberts, A. Said, H. Sinn, D. Shu, S. Stoupin, M. Upton, M. Wieczorek, and H. Yavas, J. Electron Spectrosc. Relat. Phenom. **188**, 140 (2013).
[36] P01 high resolution dynamics beamline, desy, http://photon-science.desy.de/facilities/petra_iii/beamlines/p01_dynamics/index_eng.html.
[37] Y.-D. Chuang, J. Pepper, W. McKinney, Z. Hussain, E. Gullikson, P. Batson, D. Qian, and M. Z. Hasan, J. Phys. Chem. Solids **66**, 2173 (2005).
[38] Y.-D. Chuang, L. A. Wray, J. Denlinger, and Z. Hussain, Synchrotron Radiat. News **25**, 23 (2012).
[39] L. A. Wray, S.-W. Huang, I. Jarrige, K. Ikeuchi, K. Ishii, J. Li, Z. Qiu, Z. Hussain, and Y.-D. Chuang, Frontiers Phys. **3**, 32 (2015).
[40] E. Augustin, H. He, L. Miao, Y.-D. Chuang, Z. Hussain, and L. A. Wray, J Electron Spectros Relat Phenomena **220**, 121 (2016).
[41] J. J. Lee, B. Moritz, W. S. Lee, M. Yi, C. J. Jia, A. P. Sorini, K. Kudo, Y. Koike, K. J. Zhou, C. Monney, V. Strocov, L. Patthey, T. Schmitt, T. P. Devereaux, and Z. X. Shen, Phys. Rev. B **89**, 041104(R) (2014).
[42] L. A. Wray, S.-W. Huang, Y. Xia, M. Z. Hasan, C. Mathy, H. Eisaki, Z. Hussain, and Y.-D. Chuang, Phys. Rev. B **91**, 035131 (2015).
[43] H. Ikeno, F. M. F. de Groot, E. Stavitski, and I. Tanaka, J. Phys.: Condens. Matter **21**, 104208 (2009).
[44] F. de Groot, Coord. Chem. Rev. **249**, 31 (2005).
[45] See Supplemental Material at http://link.aps.org/supplemental/10.1103/PhysRevB.99.115120 for the extraction method of

the crystal field parameters from the experimental *dd* energy positions.

[46] C. J. Jia, C.-C. Chen, A. Sorini, B. Moritz, and T. Devereaux, New J. Phys. **14**, 113038 (2012).

[47] P. Kuiper, J. H. Guo, C. Såthe, L.-C. Duda, J. Nordgren, J. J. M. Pothuizen, F. M. F. de Groot, and G. A. Sawatzky, Phys. Rev. Lett. **80**, 5204 (1998).

[48] J. Riera and A. Dobry, Phys. Rev. B **51**, 16098 (1995).

[49] M. Nishi, O. Fujita, and J. Akimitsu, Phys. Rev. B **50**, 6508 (1994).

[50] A. Abragam and B. Bleaney, *Electron Paramagnetic Resonance of Transition Ions*, International Series of Monographs on Physics (Clarendon, London, 1970).